Chemosphere 194 (2018) 275–284

Contents lists available at ScienceDirect

Chemosphere

journal homepage: www.elsevier.com/locate/chemosphere

Seasonal variations of C_1-C_4 alkyl nitrates at a coastal site in Hong Kong: Influence of photochemical formation and oceanic emissions

Junwei Song [a], Yingyi Zhang [a], Yu Huang [b, c], Kin Fai Ho [d], Zibing Yuan [a], Zhenhao Ling [e], Xiaojun Niu [a], Yuan Gao [b], Long Cui [b], Peter K.K. Louie [f], Shun-cheng Lee [b, **], Senchao Lai [a, *]

[a] Guangdong Provincial Key Laboratory of Atmospheric Environment and Pollution Control, School of Environment and Energy, South China University of Technology, Guangzhou, China
[b] Department of Civil and Environmental Engineering, The Hong Kong Polytechnic University, Hung Hom, Hong Kong
[c] Key Lab of Aerosol Chemistry & Physics, Institute of Earth Environment, Chinese Academy of Sciences, Xi'an, China
[d] The Jockey Club School of Public Health and Primary Care, The Chinese University of Hong Kong, Sha Tin, Hong Kong
[e] School of Environmental Science and Engineering, Sun Yat-sen University, Guangzhou, China
[f] Hong Kong Environmental Protection Department, Wan Chai, Hong Kong

HIGHLIGHTS

- Ambient levels of C_1-C_4 alkyl nitrates ($RONO_2$) were measured in four selected months at a coastal site.
- C_2-C_4 $RONO_2$ peaked in winter and were mainly produced via photochemical formation.
- Methyl nitrate ($MeONO_2$) peaked in summer and was mainly derived from oceanic emissions.
- The notable enrichment of $MeONO_2$ over C_2-C_4 $RONO_2$ was influenced by the oceanic air masses from the South China Sea.

ARTICLE INFO

Article history:
Received 24 July 2017
Received in revised form
14 November 2017
Accepted 19 November 2017
Available online 21 November 2017

Handling Editor: Keith Maruya

Keywords:
Alkyl nitrates
Seasonality
Photochemical production
Marine emissions
Ozone

ABSTRACT

Five C_1-C_4 alkyl nitrates ($RONO_2$) were measured at a coastal site in Hong Kong in four selected months of 2011 and 2012. The total mixing ratios of C_1-C_4 $RONO_2$ (Σ_5RONO_2) ranged from 15.4 to 143.7 pptv with an average of 65.9 ± 33.0 pptv. C_3-C_4 $RONO_2$ (2-butyl nitrate and 2-propyl nitrate) were the most abundant $RONO_2$ during the entire sampling period. The mixing ratios of C_3-C_4 $RONO_2$ were higher in winter than those in summer, while the ones of methyl nitrate ($MeONO_2$) were higher in summer than those in winter. Source analysis suggests that C_2-C_4 $RONO_2$ were mainly derived from photochemical formation along with biomass burning (58.3–71.6%), while ocean was a major contributor to $MeONO_2$ (53.8%) during the whole sampling period. The photochemical evolution of C_2-C_4 $RONO_2$ was investigated, and found to be dominantly produced by the parent hydrocarbon oxidation. The notable enrichment of $MeONO_2$ over C_3-C_4 $RONO_2$ was observed in a summer episode when the air masses originating from the South China Sea (SCS) and $MeONO_2$ was dominantly derived from oceanic emissions. In order to improve the accuracy of ozone (O_3) prediction in coastal environment, the relative contribution of $RONO_2$ from oceanic emissions versus photochemical formation and their coupling effects on O_3 production should be taken into account in future studies.

1. Introduction

Alkyl nitrates ($RONO_2$) are usually considered as a component of total reactive nitrogen ($NO_y = NO_x + HNO_3 + NO_3 + N_2O_5 +$ organic nitrates) (Day et al., 2003). They can serve as a temporary reservoir of NO_x and transport long distance because of their relatively low reactivity (Atkinson et al., 2006; Ling et al., 2016).

It has long been proposed that $RONO_2$ are mainly formed by the photochemical oxidation of hydrocarbons (e.g., methane, ethane, propane etc.) in the presence of NO_x (Atkinson et al., 2006). The photochemical formation pathways of C_1-C_4 $RONO_2$ are demonstrated as follows (Arey et al., 2001; Atkinson et al., 2006):

* Corresponding author.
** Corresponding author.
E-mail addresses: ceslee@polyu.edu.hk (S.-c. Lee), sclai@scut.edu.cn (S. Lai).

https://doi.org/10.1016/j.chemosphere.2017.11.104
0045-6535/

$$RH + {}^{\bullet}OH \rightarrow {}^{\bullet}R + H_2O,\ k_1,\ \alpha_1 \quad (R1)$$

$${}^{\bullet}R + O_2 \rightarrow {}^{\bullet}RO_2,\ k_2 \quad (R2)$$

$${}^{\bullet}RO_2 + NO \rightarrow {}^{\bullet}RO + NO_2,\ k_3,\ 1\text{-}\alpha_2 \quad (R3)$$

$${}^{\bullet}RO_2 + NO \rightarrow {}^{\bullet}RONO_2,\ k_4,\ \alpha_2 \quad (R4)$$

$${}^{\bullet}RO + NO_2 \rightarrow {}^{\bullet}RONO_2,\ k_5 \quad (R5)$$

$$NO_2 + O_2 \rightarrow NO + O_3,\ k_6 \quad (R6)$$

where k_1, k_2, k_3, k_4 *and* k_5 are the reaction rate constants; α_1 and α_2 are the branching ratios for the Reactions (R1) and (R4) of parent hydrocarbons (RH) with hydroxyl radicals (•OH) and peroxyl radicals ($^{\bullet}RO_2$) with NO, respectively. Briefly, alkyl radicals (•R) result from the •OH-initiated oxidation of RH (R1) and can subsequently react with O_2 to form $^{\bullet}RO_2$ (R2). A large fraction of $RONO_2$ is usually formed via reaction of $^{\bullet}RO_2$ with NO (R4) (Atkinson et al., 1982; Bertman et al., 1995). Another branch of reaction of $^{\bullet}RO_2$ with NO can produce alkoxy radicals (•RO) and NO_2 (R3), leading to the alternative formation pathway of $RONO_2$ through the reaction of •RO and NO_2 (R5) (Flocke et al., 1998a, 1998b). In addition to secondary photochemical formation, primary emissions of C_1-C_3 $RONO_2$ from the oceans (Atlas et al., 1993; Blake et al., 2003; Ling et al., 2016) and biomass burning (Simpson et al., 2002) have been reported previously. However, other emissions are not considered as important sources of C_1-C_3 $RONO_2$ (Perring et al., 2013). Ambient observations over the equatorial Pacific showed that the levels of C_1-C_2 $RONO_2$ were enhanced in this region (Atlas et al., 1993; Blake et al., 2003). Direct measurements of $RONO_2$ in seawater showed that C_1-C_3 $RONO_2$ can be supersaturated in surface layer (Chuck et al., 2002; Moore and Blough, 2002; Dahl et al., 2007). These results indicated that oceanic emissions are a source of $RONO_2$ in the atmosphere. In contrast, the removal of $RONO_2$ primarily includes photolysis and the reaction with •OH (Clemitshaw et al., 1997; Talukdar et al., 1997a, 1997b).

$$RONO_2 \xrightarrow{h\nu} \cdot RO + NO_2,\ J_{RONO_2} \quad (R7)$$

$$RONO_2 + \cdot OH \rightarrow \text{products},\ k_6 \quad (R8)$$

where *hv* is sunlight; J_{RONO2} and k_6 are the rate constants of photolysis and •OH reaction, respectively. Photolysis is the dominant mechanism for the removal of C_1-C_3 $RONO_2$, while •OH reaction is more important for the removal of $RONO_2$ with carbon number higher than 4 (Clemitshaw et al., 1997; Talukdar et al., 1997a, 1997b). Besides, Russo et al. (2010) and Wu et al. (2011) suggested that dry deposition is another removal process for $RONO_2$.

Photochemical $RONO_2$ are the byproducts of ozone (O_3) formation through the reactions between volatile organic compounds (VOCs) and NO_x (Lyu et al., 2017). Photochemical formation of $RONO_2$ involves the oxidation of NO to NO_2 (R3), promoting the production of O_3 (R6). Meanwhile, the formation reaction (R5) could reduce the budget of NO_2 by directly competing with the formation of O_3 (R6). In addition, as temporary nitrogen reservoirs, the photolysis of $RONO_2$ could also release NO_2 (R7), increasing the potential of O_3 formation. Therefore, there is a complex and close association between $RONO_2$ and O_3 (Lyu et al., 2017). Recently, modeling studies have reported that the formation and degradation of photochemical $RONO_2$ have significant impacts on O_3 production (Lyu et al., 2015, 2017; Ling et al., 2016). Additionally, Neu et al. (2008) proposed that C_1-C_2 $RONO_2$ from oceanic emissions could subsequently produce NO_2 through photolysis, contributing to the budgets of tropospheric NO_x and O_3.

C_1-C_4 $RONO_2$ have been widely studied at different geographical locations, including remote marine (Atlas et al., 1993; Schneider and Ballschmiter, 1999; Blake et al., 2003), coastal (Simpson et al., 2006; Russo et al., 2010), rural (Atlas, 1988; Shepson et al., 1993) and urban areas (Wang et al., 2013; Aruffo et al., 2014; Ling et al., 2016). In the Pacific troposphere (8°N-13°S), primary oceanic emissions were suggested to be the most important sources of $RONO_2$, especially for C_1-C_2 $RONO_2$ (Blake et al., 2003). In contrast, in rural and urban areas, C_1-C_4 $RONO_2$ are mainly formed from photochemical processes, which are generally dominated in formation of C_3-C_4 $RONO_2$ (Simpson et al., 2006; Wang et al., 2013; Ling et al., 2016). However, knowledge on the relative contribution of photochemical formation and primary oceanic emissions on $RONO_2$ in coastal environment is limited (Simpson et al., 2006; Russo et al., 2010). A measurement of C_1-C_5 $RONO_2$ in coastal New England indicated that the levels of $RONO_2$ were controlled by the photochemical formation of their precursors rather than oceanic emissions (Russo et al., 2010). Another long-term measurement of C_1-C_5 $RONO_2$ at a coastal site in Hong Kong (Tai O) also showed that oceanic emissions had minor contribution to $RONO_2$ (Simpson et al., 2006). However, researchers recently investigated the distributions of C_1-C_3 $RONO_2$ on a global scale by using chemical transport models and found a large discrepancy between the modeled and observed $RONO_2$ data when oceanic emissions were absent in the models (Williams et al., 2014; Khan et al., 2015).

During last decades, rapid economic development led to severe air pollution with high concentrations of particles and O_3 in the Pearl River Delta (PRD) region, China (Lai et al., 2016; Ou et al., 2016; Ling et al., 2017), which increased atmosphric reactivity and promoted various atmospheric chemical processes in coastal and oceanic areas (Lai et al., 2016; Song et al., 2017).There were limited studies focusing on the characteristics of $RONO_2$ in this region (Simpson et al., 2006; Lyu et al., 2015; Ling et al., 2016), although they may have significant impacts on O_3 production. Here we conducted an observation of C_1-C_4 $RONO_2$ at a coastal site in Hong Kong during four selected months of May, August, November 2011 and February 2012. The aims of this work are (1) to observe the ambient levels and seasonal variations of $RONO_2$ and (2) to investigate the influence of photochemical formation and oceanic emissions on $RONO_2$ in coastal environment.

2. Methods

2.1. Sampling site

Whole air samples were collected at a coastal site of 2.3 m above ground level in Hong Kong University of Science and Technology (HKUST, 22.33°N and 114.27°E). The sampling station is located on the west of shorefront and approximately 8–10 km east of the highly developed Kowloon urban area of Hong Kong (Fig. 1). There is no major industrial emissions and little traffic near this site. It is an ideal site to study background air quality and regional transport in Hong Kong (Cheng et al., 2014; Cheung et al., 2015; Man et al., 2015).

2.2. Sampling and chemical analysis

Twenty-four hour (0:00–23:59) integrated air samples were collected using pre-treated and evacuated 2-L electro-polished stainless steel canisters by an automated sampler (Model 2200,

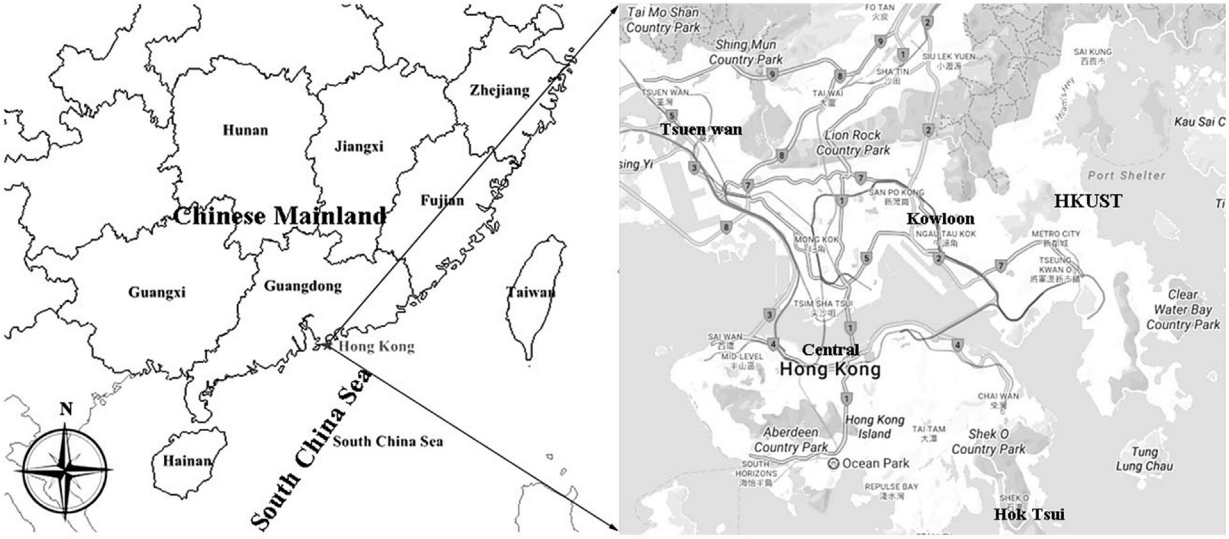

Fig. 1. Location of the sampling site, Hong Kong University of Science and Technology (HKUST).

Malibu, CA) approximately once every three days in May, August, November 2011 and February 2012. The final pressure was 29 ± 1 psi in the canisters. A 47 mm Teflon filter was placed on a holder to remove particulates from the air stream before entering the flow lines. The sampled canisters were transported to a laboratory in the University of California at Irvine (UCI) for analysis of volatile organic compounds (VOCs) within two weeks after sample collection. The stability of the target compounds was demonstrated by preparing a purified air filled canister injected with a known amount of certified gas mixture. The recovery of each target compounds was close to 100%, indicating the stability of the target VOCs during the storage and transport processes (Huang et al., 2015). The detailed descriptions of the analytical system, measurement detection limits, accuracy and precision of VOCs have been provided in the previous publications (Colman et al., 2001; Barletta et al., 2002; Simpson et al., 2006). Briefly, five $RONO_2$, i.e., methyl nitrate ($MeONO_2$), ethyl nitrate ($EtONO_2$), 2-propyl nitrate (2-$PrONO_2$), 1-propyl nitrate (1-$PrONO_2$) and 2-butyl nitrate (2-$BuONO_2$), were quantified by a gas chromatography (GC) with electron capture detector (ECD). The precision and detection limits of $RONO_2$ measurements are 5% and 0.1 pptv, respectively (Huang et al., 2015). The calibration scale for $RONO_2$ measurements changed in 2008, increasing by factors of 2.13, 1.81, 1.24 and 1.17 for the C_1, C_2, C_3, C_4 $RONO_2$, respectively (Simpson et al., 2011). Methane and other VOCs (i.e., alkanes, alkenes, ethyne, aromatics and halocarbons) were simultaneously detected by using a combination of GC with flame ionization detector (FID) and mass spectrometric detector (MSD). The accuracy of measurements is 1% for methane, 2–20% for halocarbons and 5% for other VOCs. The measurement precision is 2% for methane, 1–5% for halocarbons and 0.5–5% for other VOCs. The measurement detection limits (MDLs) of VOCs are shown in Table S1.

Auxiliary data of O_3 and NO/NO_2 were obtained from the HKUST's ENVF Atmospheric and Environmental Database. The ambient concentrations of O_3 and NO/NO_2 were determined every 5 min by a UV photometric O_3 analyzer (API, Model 400E) and a chemiluminescence $NO\text{-}NO_2\text{-}NO_x$ analyzer (API, Model 200E), respectively. The detection limits are 1 ppbv and 0.5 ppbv for O_3 and NO_2/NO_x, respectively.

2.3. Model analysis

Air mass backward trajectories were computed for the air samples using Hybrid Single Particle Lagrangian Integrated Trajectory (HYSPLIT) model (Stein et al., 2015). The HYSPLIT model uses the archived meteorological dataset from the National Oceanic and Atmospheric Administration (NOAA) Air Resources Laboratory as an input file. Three-day backward trajectories were calculated for each sampling month at an altitude of 200 m above sea level. The source profiles and contributions of $RONO_2$ were investigated by using the principle component analysis (PCA) and positive matrix factorization (PMF) model. A more detailed description of PCA and PMF is shown in supplement (Appendix A).

3. Results and discussion

3.1. Seasonal variations of alkyl nitrates

Table 1 shows the statistics of C_1-C_4 $RONO_2$ and their parent hydrocarbon mixing ratios measured at HKUST in May, August, November 2011 and February 2012. The total mixing ratios of the five $RONO_2$ (Σ_5RONO_2) ranged from 15.4 to 143.7 pptv with an average of 65.9 ± 33.0 pptv throughout the entire sampling period. The predominant $RONO_2$ was 2-$BuONO_2$ with an average level of 25.5 ± 17.8 pptv, followed by 2-$PrONO_2$ (18.9 ± 11.0 pptv), $MeONO_2$ (10.4 ± 2.9 pptv) and $EtONO_2$ (8.5 ± 3.8 pptv). Among the observations at coastal sites in Hong Kong (Fig. S1), the average levels of C_1-C_4 $RONO_2$ were comparable to those measured at Hok Tsui in spring (Wang et al., 2003), but lower than those observed at Tai O in 2001–2002 (Simpson et al., 2006). All these mixing ratios of C_1-C_4 $RONO_2$ in our study were higher than the values reported in coastal New England (Russo et al., 2010), and lower than those obtained in urban environments, such as Tsuen Wan, Hong Kong (Ling et al., 2016) and other Chinese urban sites (Wang et al., 2013). The dominance of C_3-C_4 $RONO_2$ (2-$BuONO_2$ and 2-$PrONO_2$) over C_1-C_2 $RONO_2$ at HKUST was similar with those reported in the previous studies (Simpson et al., 2006; Russo et al., 2010; Wang et al., 2013; Ling et al., 2016). It can be ascribed to the increasing branching ratios of photochemical $RONO_2$ production

Table 1
Mixing ratios of C_1-C_4 $RONO_2$, their parent hydrocarbons and meteorological parameters measured at HKUST in May, August, November 2011 and February 2012.

Species	Entire sampling period		Summer	Winter
	mean	range	mean	mean
$RONO_2$ (pptv)				
$MeONO_2$	10.4 ± 2.9	5.8–18.2	12.0 ± 2.9	8.8 ± 1.9
$EtONO_2$	8.5 ± 3.8	1.8–17.3	7.2 ± 4.1	9.8 ± 3.1
2-$PrONO_2$	18.9 ± 11.0	2.0–43.7	11.7 ± 8.3	26.1 ± 8.4
1-$PrONO_2$	2.5 ± 1.6	0.5–6.9	1.8 ± 1.4	3.3 ± 1.4
2-$BuONO_2$	25.5 ± 17.8	2.1–66.9	13.5 ± 11.0	37.6 ± 15.0
Σ_5RONO_2	65.9 ± 33.0	15.4–143.7	46.1 ± 25.4	85.6 ± 27.7
Parent hydrocarbons (pptv)				
Methane (ppmv)	1.96 ± 0.08	1.80–2.14	1.97 ± 0.11	1.95 ± 0.04
Ethane	1751 ± 1274	236–4937	831 ± 613	2672 ± 1083
Propane	1070 ± 690	108–2657	671 ± 499	1470 ± 625
n-Butane	763 ± 491	178–2502	767 ± 631	759 ± 309
Meteorological parameters				
Temperature (°C)	23.6 ± 5.6	12.3–30.9	28.1 ± 2.2	19.1 ± 4.2
Relative humidity (%)	79 ± 8	60–99	78 ± 7	80 ± 9
Wind speed (m/s)	5.7 ± 2.7	1.7–13.0	4.0 ± 1.6	7.5 ± 2.4

with the increasing carbon numbers (Atkinson et al., 1982), although the mixing ratios of their parent hydrocarbons should decrease with the increasing carbon numbers. The average mixing ratios of C_3-C_4 parent hydrocarbons (i.e., propane and *n*-butane) were lower than C_1-C_2 parent hydrocarbons (i.e., methane and ethane). It suggests the importance of photochemical production for C_3-C_4 $RONO_2$ in our observation. The mixing ratios of 1-$PrONO_2$ were much lower than 2-$PrONO_2$ due to the lower photochemical branching ratio of 1-$PrONO_2$ (Atkinson et al., 1982).

In Hong Kong, May and August represent summer months, and November and February represent winter months (Lee et al., 2002; Guo et al., 2004). In this study, the average levels of C_3-C_4 $RONO_2$ in winter were higher than those in summer by factors of 2–3. However, $MeONO_2$ showed an opposite seasonal trend with significantly higher levels in summer than those in winter ($p = 0.015$, two-tailed *t*-test). Besides, there was no significant difference in the levels of $EtONO_2$ between the two seasons ($p = 0.102$). At Tai O, Hong Kong, Simpson et al. (2006) found a similar seasonality of C_3-C_4 $RONO_2$ with maximum in winter and minimum in summer. Russo et al. (2010) also observed higher C_3-C_4 $RONO_2$ levels in winter than those in summer in coastal New England, whereas C_1-C_2 $RONO_2$ showed a homogenous distribution throughout the year. The seasonality of $RONO_2$ can be constrained by several factors including their sources and sinks, as well as the seasonal transport patterns (Simpson et al., 2006; Russo et al., 2010). Due to the higher OH radical concentration and faster photolysis reactions, C_3-C_4 $RONO_2$ can be removed more quickly in summer (Clemitshaw et al., 1997; Talukdar et al., 1997b; Atkinson et al., 2006). On the other hand, C_3-C_4 $RONO_2$ photochemical yields are temperature dependent, increasing with the decreasing temperature (Atkinson et al., 1983). In our study, the average temperature was lower in winter (19.1 ± 4.2 °C) than in summer (28.1 ± 2.2 °C). These factors in photochemical processes can explain the seasonal variations of C_3-C_4 $RONO_2$.

Due to the Asian monsoon system, the prevailing winds in Hong Kong are from northeast in winter and from south in summer, respectively (Simpson et al., 2006). In our study, the backward trajectory analysis shows that the air masses frequently traveled across the Chinese mainland in winter and the South China Sea (SCS) in summer (Fig. 2). Since $RONO_2$ had relatively long lifetime (Clemitshaw et al., 1997; Talukdar et al., 1997a;

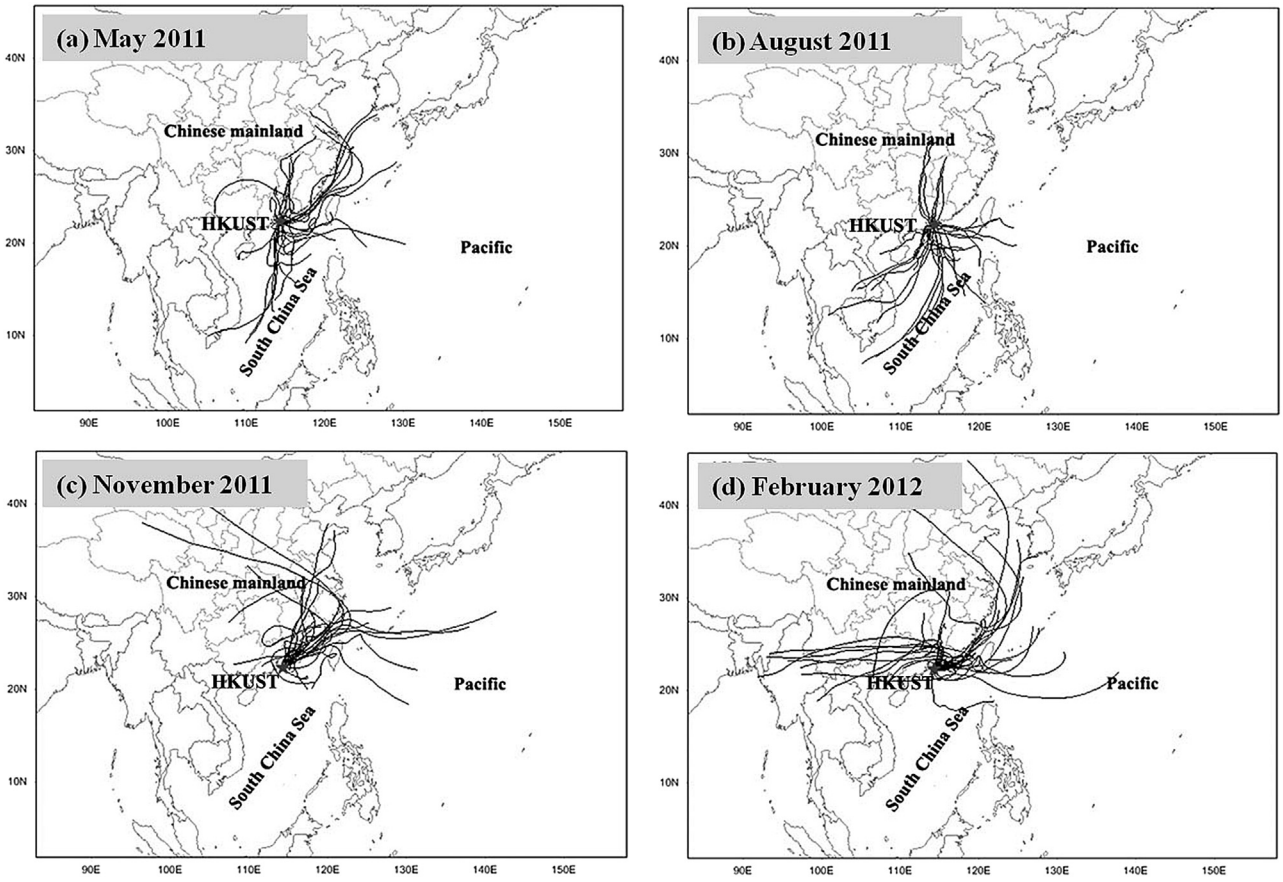

Fig. 2. Three-day backward air mass trajectories were calculated in the month of (a) May 2011, (b) August 2011, (c) November 2011 and (d) February 2012 at HKUST.

Atkinson et al., 2006), high levels of $RONO_2$ can be transported from the Chinese mainland to this site in winter. In summer, clean oceanic air masses may efficiently dilute the levels of $RONO_2$. As expected, the seasonal variations for C_3-C_4 $RONO_2$ were similar to those for CO and anthropogenic VOCs, e.g., benzene, toluene (Table S1). In contrast, $MeONO_2$ showed a similar seasonal variation with dimethyl sulfide (DMS), a specific tracer for oceanic emissions (Nowak et al., 2001). The enhancement of $MeONO_2$ in summer was likely related to the oceanic emissions, which has already been suggested by previous studies (Chuck et al., 2002; Moore and Blough, 2002; Blake et al., 2003).

3.2. Source attribution of alkyl nitrates

In both summer and winter, C_2-C_3 $RONO_2$ showed strong positive correlations with 2-$BuONO_2$ (r^2 = 0.58–0.95, Fig. S2), which was believed to be entirely produced by *n*-butane photochemical oxidation (Bertman et al., 1995). However, no significant correlations were found between $MeONO_2$ and 2-$BuONO_2$ in both seasons ($p > 0.05$), suggesting the different sources or formation processes of $MeONO_2$. The levels of methane were comparable between the two seasons (1.97 ± 0.11 ppmv in summer and 1.95 ± 0.04 ppmv in winter). Based on the kinetics of methane ($k_{CH4+OH} = 6.2 \times 10^{-15}$ cm^3 $molecule^{-1}$ s^{-1} at 298 K) (Atkinson, 1997), the yield of $MeONO_2$ from methane oxidation was estimated below 1 pptv in 1 day for methane of 2 ppmv given at diurnal OH radicals of 2×10^6 molecule cm^{-3}. These results suggest that the oxidation of methane was not the major source for $MeONO_2$.

Previous studies have suggested the possible additional formation pathways of $MeONO_2$, including (1) the reaction of methoxy radicals ($\cdot CH_3O$) with NO_2 (Simpson et al., 2006), (2) the reaction of methanol with nitric acid (HNO_3) (Fan et al., 1994), (3) the decomposition of larger compounds, e.g., larger alkoxy radicals and peroxyacetyl nitrate (PAN) (Flocke et al., 1998b; Simpson et al., 2003; Worton et al., 2010). The first two pathways have been proven to be insignificant under most of the atmospheric conditions (Orlando et al., 1992; Simpson et al., 2006; Iraci et al., 2007; Lyu et al., 2015). The decomposition of larger compounds could be a potential source of methyl peroxy radicals ($\cdot CH_3O_2$), contributing to $MeONO_2$ via reaction of $\cdot CH_3O_2$ with NO ($\cdot CH_3O_2 + NO \rightarrow CH_3ONO_2$) (Flocke et al., 1998a). Here we use the maximum value of PAN with 5 ppbv based on an observation in Hong Kong in the same period of our study (summer of 2011) to estimate the concentration of $MeONO_2$ from PAN decomposition (Xu et al., 2015). Assuming that all the PAN are converted to produce $\cdot CH_3O_2$ reacting with NO to form $MeONO_2$, the concentration of $MeONO_2$ from the decomposition of PAN can be roughly estimated as follows:

$$\frac{d[MeONO_2]}{d[t]} = \alpha k[\cdot CH_3O_2][NO]$$

where k is the reaction rate coefficient of 6.9×10^{-13} cm^3 $molecule^{-1}$ s^{-1}, and α is the branching ratio of 0.0003 (Flocke et al., 1998a). $[MeONO_2]$, $[\cdot CH_3O_2]$ and [NO] represent the concentrations of $MeONO_2$, $\cdot CH_3O_2$ and NO, respectively. According to the maximum value of NO (45 ppbv) and PAN (5 ppbv) in August (Xu et al., 2015), the yield of $MeONO_2$ can be estimated to be 4×10^{-3} pptv in 1 day from PAN decomposition, which was much lower than those observed in August.

In order to explore the sources of $RONO_2$, we performed a principal component analysis (PCA) on the measured data of C_1-C_4 $RONO_2$, CO, CH_3Cl and DMS during the entire sampling period (Fig. S3). Two principal components (PC1 and PC2) can explain totally 84.2% of the variation. PC1 explains 66.4% of the variation with high loadings of C_2-C_4 $RONO_2$, CO and CH_3Cl. CO was considered as a tracer of combustion processes (Lai et al., 2010, 2011) and CH_3Cl was selected as a tracer of biomass burning (Simpson et al., 2011). Therefore, PC1 was characterized with photochemical formation and biomass burning. PC2 explains 17.8% of the variation with high loadings of $MeONO_2$ and DMS (a specific tracer for oceanic emissions) (Nowak et al., 2001). Given the location of HKUST is adjacent to the SCS, it is highly possible that PC2 was associated with the oceanic emissions. Furthermore, a PMF model was further used to estimate the source profiles and contributions to individual $RONO_2$. As shown in Fig. 3, the first factor is distinguished by high loadings of C_2-C_4 $RONO_2$. In addition, this factor includes moderate to high percentages of CO, CH_3Cl, ethyne and ethane, which were mainly derived from biomass burning (Lai et al., 2010, 2011; Simpson et al., 2011). Therefore, this factor is identified as the sources of photochemical formation and biomass burning. The second factor is dominated by the significant presence of DMS, CH_4 and $MeONO_2$, which were associated with the oceanic emissions. The third factor is distinguished by high percentages of propane, *i*-butane and *n*-butane, which are the typical tracers for liquefied petroleum gas (LPG) usage (Guo et al., 2007). During the whole sampling period, the contribution of photochemical formation together with biomass burning to $EtONO_2$, 2-$PrONO_2$, 1-$PrONO_2$ and 2-$BuONO_2$ are 58.3%, 71.2%, 67.4% and 71.6%, respectively. Therefore, ocean is the dominant contributor to $MeONO_2$ (53.8%) and to some extent contributes to $EtONO_2$ (21.6%). Besides, the contributions of LPG usage to individual $RONO_2$ range from 20.1% to 27.1%.

3.3. Photochemical evolution of C_2-C_4 alkyl nitrates

Bertman et al. (1995) developed a simplified reaction model to evaluate the photochemical processing of $RONO_2$, which has been applied in many studies (Roberts et al., 1998; Simpson et al., 2003; Reeves et al., 2007; Russo et al., 2010; Worton et al., 2010; Wang et al., 2013; Ling et al., 2016). Briefly, it assumes that: (1) the Reaction (R1) of RH with $\cdot OH$ is the rate-limiting step for $RONO_2$ photochemical formation and (2) the environment is NO_x-rich (>0.1 ppbv), making the Reaction (R4) is the dominant pathway for $\cdot RO_2$ removal (Roberts et al., 1998). In this study, the

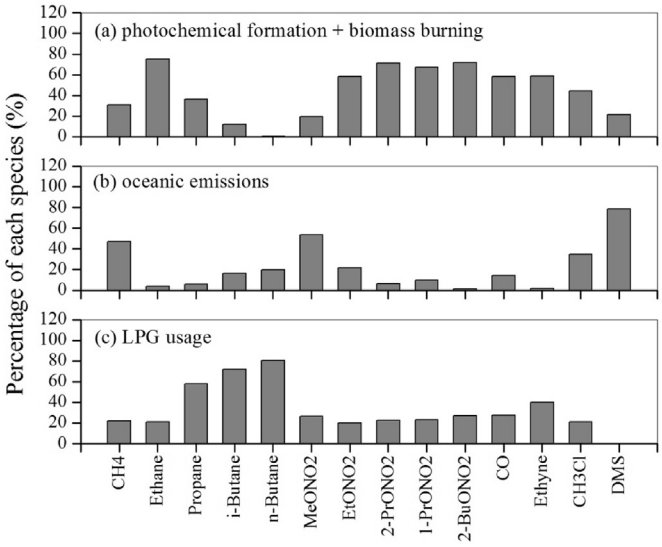

Fig. 3. Factor profiles (percentages of each species) resolved by PMF model at HKUST during the entire sampling period.

average mixing ratio of NO_x (8.0 ± 5.7 ppbv) was high enough so that $•RO_2$ was predominantly removed by its reaction with NO. Then the photochemical reaction schemes (R1-R7) could be simplified as follows:

$$RH \xrightarrow{k_A,\beta} RONO_2 \xrightarrow{k_B} products \quad (R9)$$

The photochemical evolution (R8) can be expressed as a function with reaction time (t):

$$\frac{[RONO_2]}{[RH]} = \frac{\beta k_A}{k_B - k_A(1 - e^{(k_B - k_A)t})} + \frac{[RONO_2]_0}{[RH]_0} e^{(k_B - k_A)t}$$

where $\beta = \alpha_1\alpha_4$, $k_A = k_1[•OH]$ and $k_B = k_4[•OH] + J_{RONO2}$ are the pseudo-first order rate constants for $RONO_2$ production and removal. The kinetics of α_1, α_4, k_1, k_4 and J_{RONO2} are obtained from the published literature (Table S2) (Bertman et al., 1995; Kwok and Atkinson, 1995; Clemitshaw et al., 1997; Roberts et al., 1998; Arey et al., 2001; Simpson et al., 2003; Atkinson et al., 2006). [•OH] is the average concentration of •OH. Based on the studies in the PRD region (Simpson et al., 2003; Hofzumahaus et al., 2009), the values of 2×10^6 and 1×10^6 molecules cm^{-3} are assumed for [•OH] in summer and winter, respectively. $[RONO_2]_0$ and $[RH]_0$ represent the initial levels of $RONO_2$ and RH before photochemical processing. Typically, $[RONO_2]_0/[RH]_0$ equal to zero was adopted for modeling the photochemical evolution (Bertman et al., 1995; Roberts et al., 1998; Simpson et al., 2003; Worton et al., 2010), while more recent studies have proposed to use non-zero $[RONO_2]_0/[RH]_0$ to evaluate the influence of background levels (Russo et al., 2010; Wang et al., 2013; Ling et al., 2016). In this study, we assume that the non-zero $[RONO_2]_0/[RH]_0$ is equal to the lowest seasonal $[RONO_2]/[RH]$ value.

The observed $RONO_2$/RH ratios were plotted against another $RONO_2$/RH ratios with comparisons to the photochemical evolution curves calculated from kinetics. As shown in Fig. 4, the ratios of 2-$BuONO_2$/*n*-butane were plotted on the abscissa because 2-$BuONO_2$ was predominantly produced from *n*-butane photochemical oxidation (Bertman et al., 1995). The given time of photochemical evolution ranged from 1 min to 10 days. As a result of the influence of $[RONO_2]_0/[RH]_0$, the non-zero $[RONO_2]_0/[RH]_0$ curves varied significantly with the zero $[RONO_2]_0/[RH]_0$ curves, especially at shorter processing time (<1 day). In winter (Fig. 4b), the observed values of C_2-C_3 $RONO_2$/RH were mostly close to the modeled curves with non-zero $[RONO_2]_0/[RH]_0$, indicating that photochemical formation from ethane and propane oxidation contributed significantly to C_2-C_3 $RONO_2$. However, the observed ratios of C_2-C_3 $RONO_2$/RH were higher than the zero $[RONO_2]_0/[RH]_0$ curves by factors of ~2–15. It indicates that the influence of background $RONO_2$ and RH levels should be taken into account. In summer (Fig. 4a), the observed ratios of C_2-C_3 $RONO_2$/RH to 2-$BuONO_2$/*n*-Butane followed the trends of non-zero $[RONO_2]_0/[RH]_0$ curves, but we found that the observed C_2-C_3 $[RONO_2]/[RH]$

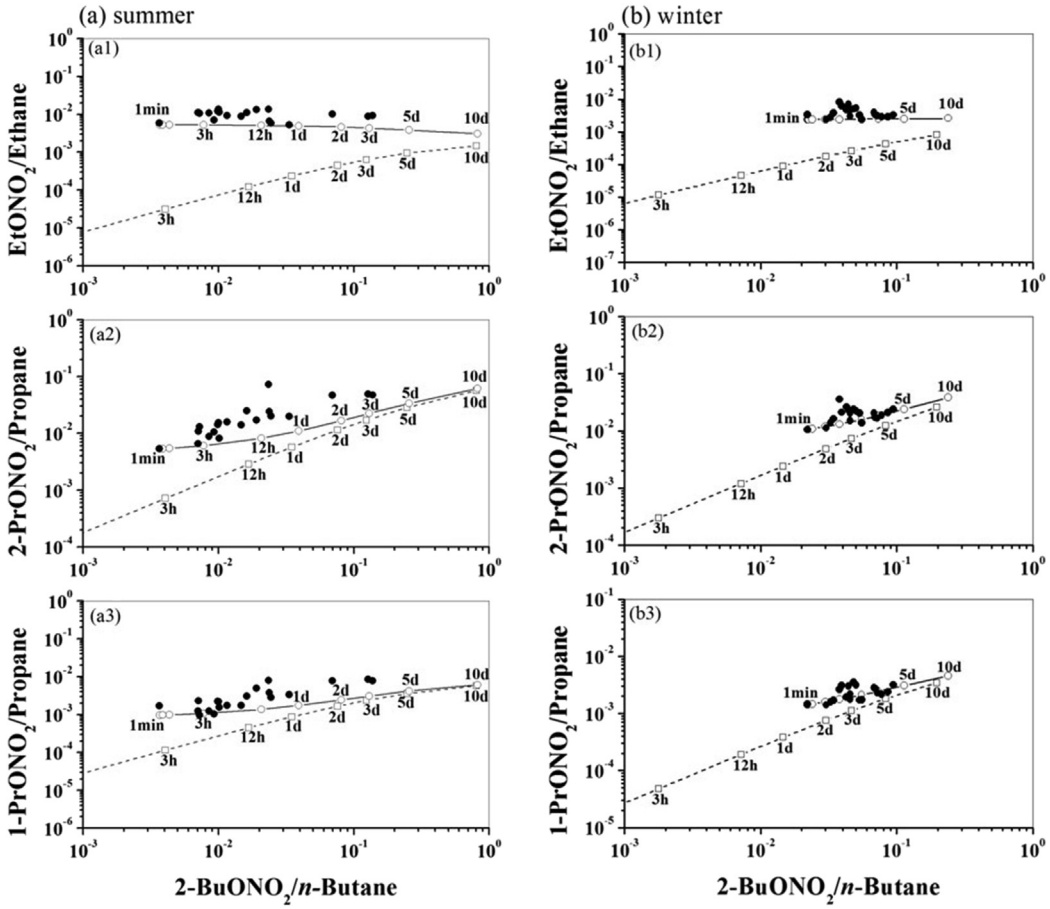

Fig. 4. Photochemical evolutions of C_2-C_3 $RONO_2$/RH versus 2-$BuONO_2$/*n*-Butane. The solid circles represent the observed ratios in: (a) summer and (b) winter. The dash and solid curves represent the photochemical evolution curves, plotting on the basis of $[RONO_2]_0/[RH]_0 = 0$ and non-zero $[RONO_2]_0/[RH]_0$ with the lowest seasonal $[RONO_2]/[RH]$, respectively. The given photochemical evolution time ranged from 1 min to 10 days (open circles).

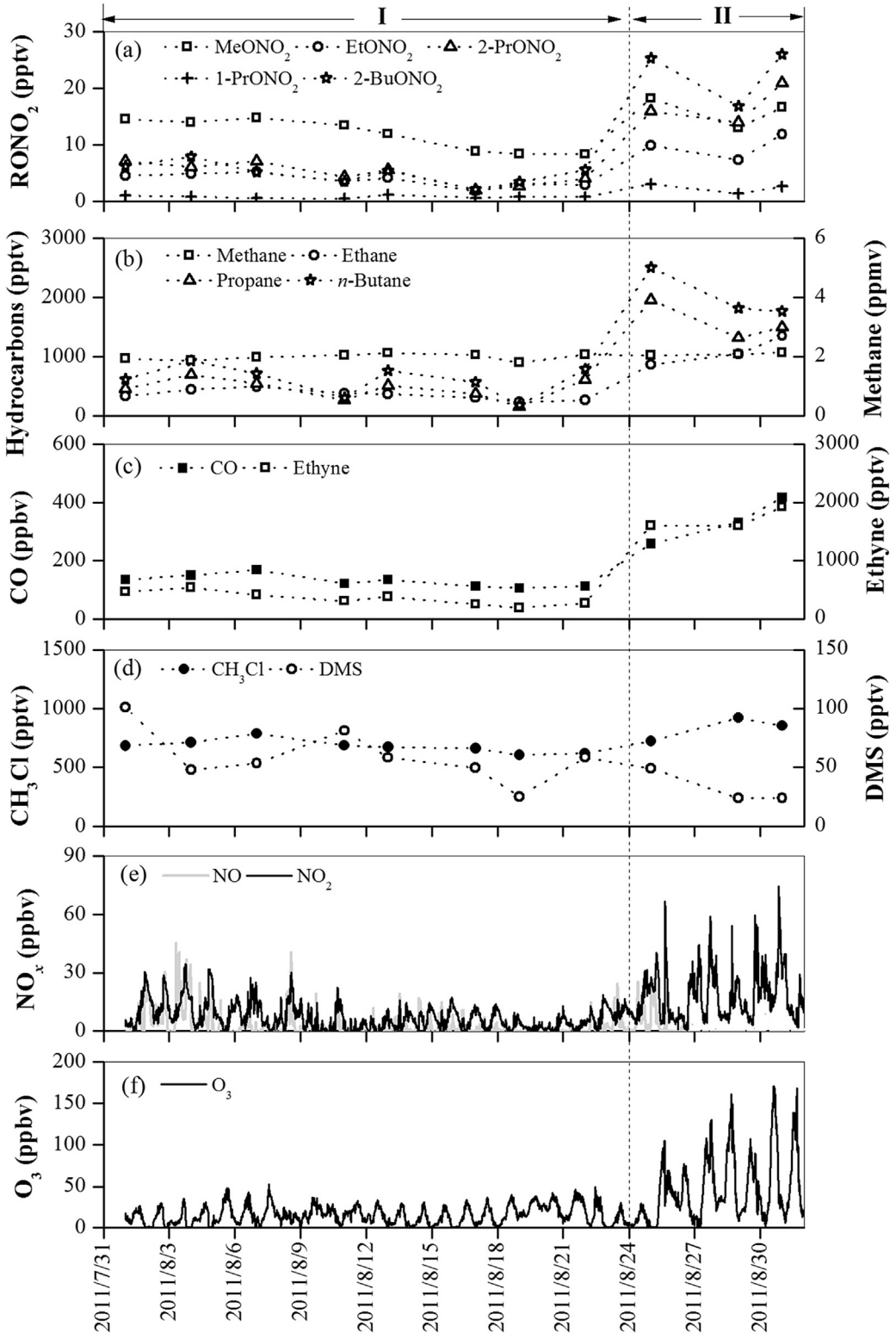

Fig. 5. Temporal variations of (a) $RONO_2$, (b) hydrocarbons, (c) CO and ethyne, (d) CH_3Cl and DMS, (e) NO_x and (f) O_3 in summer episodes (August 2011).

were higher than these modeled curves. It should be noted that this simplified model may contain some uncertainties. The seasonal wind patterns have a significant impact on $RONO_2$ and RH levels. This will likely affect the values of $[RONO_2]_0/[RH]_0$, changing the position of the modeled curves.

3.4. Oceanic emissions versus photochemical formation in a summer month

In the Pacific Ocean (8°N-13°S), Blake et al. (2003) suggested that oceanic emissions of C_1-C_2 $RONO_2$ could be estimated by a

$MeONO_2/EtONO_2$ ratio of approximately 3–4, while air masses influenced by urban emissions lead to much lower $MeONO_2/EtONO_2$ ratios. In our study, the ratios of $MeONO_2/EtONO_2$ ranged from 0.6 to 1.6 in winter, indicating the influence of urban emissions, which is consistent with the backward trajectory analysis (Fig. 2). In summer, $MeONO_2/EtONO_2$ ratios fluctuated from 0.8 to 4.9, which could be due to the alternative influence of oceanic and continental air masses. In order to better understand the influence of air masses with different sources on $RONO_2$, we selected the month of August and classified it into two Episodes (Fig. 5) based on the backward trajectories: Episode I with the air masses from the SCS (1–22 August, $n = 8$) and Episode II with the continental outflow from Chinese mainland (25–31 August, $n = 3$). In the first Episode, the observed ratios of $MeONO_2/EtONO_2$ ranged from 2.7 to 4.9 in Episode I, close to that of oceanic emissions (3–4) (Blake et al., 2003). Besides, the mixing ratios of $MeONO_2$ were higher than those of C_2-C_4 $RONO_2$ in this Episode, and contributed to $\Sigma_5 RONO_2$ ranging from 38.6 to 57.7%. It suggests that oceanic emissions may play an important role in $RONO_2$ variations in this Episode. In Episode II, the ratios of $MeONO_2/EtONO_2$ (1.4–1.8) were significantly lower than those in Episode I. The mixing ratios of C_3-C_4 $RONO_2$ were higher than those of $MeONO_2$ in Episode I, suggesting that the influence of photochemical formation became more important to $RONO_2$. Although the levels of $MeONO_2$ increased slightly from Episode I to II, there was no significant difference of $MeONO_2$ between the two Episodes ($p = 0.087$).

Similar variations were observed for CO and ethyne with C_2-C_4 $RONO_2$ and their parent hydrocarbons (Fig. 5a–c). It suggests the dilution of oceanic air masses and the contribution of continental outflow to these species in Episode I and II, respectively. The ratio of ethyne/CO can be used to evaluate the age of air masses, increasing from <1 pptv/ppbv for very processed air to 4–5 pptv/ppbv for fresh polluted air (Smyth et al., 1996). Guo et al. (2007) reported the ethyne/CO ratios of 5.6–7.5 pptv/ppbv for fresh sources in Hong Kong. The ethyne/CO ratios ranged from 1.8 to 3.6 pptv/ppbv with an average of 2.7 ± 0.6 pptv/ppbv in Episode I, lower than those in Episode II (4.6–6.2 pptv/ppbv with an average of 5.2 ± 0.9 pptv/ppbv). Lower ethyne/CO ratios suggest that the air masses arriving at HKUST were aged in Episode I. It should be noted that $MeONO_2$ could be more enriched than C_2-C_4 $RONO_2$ in the aged continental air masses due to its longer lifetime. Ding et al. (2004) reported that the sea-breezes could bring the daytime photochemical pollutants from land and recirculation over the ocean to the coastal region at night. However, we did not find the changes of air mass origins in Episode I (Fig. S4). Therefore, the influence of aged continental plumes via recirculation over the SCS was negligible on $RONO_2$.

We found a good correlation between $MeONO_2$ and CH_3Cl ($r^2 = 0.69$, $p < 0.05$) in Episode I, suggesting the contribution of biomass burning (Simpson et al., 2002) and/or oceanic emissions (Rasmussen et al., 1980). Although some air masses in August were derived from the Southeast Asia (SEA) and passed over the SCS (Fig. 2 and Fig. S4), there were few fire spots observed in these regions (Fig. S5). Besides, the levels of species (e.g., CO, ethane, ethene and ethyne) associated with biomass burning were also in low levels during Episode I. It suggests that oceanic emissions were the major sources of $MeONO_2$ rather than biomass burning in this Episode. This is also supported by the variation of DMS, which was approximately 2-fold higher in Episode I than II (Fig. 4e). Although no significant correlation was found between $MeONO_2$ and DMS in Episode I ($p > 0.05$), it was possibly because DMS production was not related to the same sources that contribute to $MeONO_2$ (Blake et al., 2003). Additionally, the different lifetimes of $MeONO_2$ and DMS (only a few hours) (Barnes et al., 2006) may deteriorate the correlation between $MeONO_2$ and DMS.

In addition, relatively high levels of O_3, NO_2 and C_2-C_4 parent hydrocarbons were observed in Episode II showing similar variations with those of C_2-C_4 $RONO_2$. This similar trends between O_3 and C_2-C_4 $RONO_2$ were also observed in other months (Fig. S6-S8). Previous studies have shown that $RONO_2$ and O_3 are photochemical co-products involving VOCs and NO_x sharing a common formation mechanism. Recent applications of the photochemical box model with Master Chemical Mechanism (PBM-MCM) from intensive measurement during pollution episodes reported that the photochemical formation of $RONO_2$ exert a negative impact on O_3 production (Lyu et al., 2015, 2017; Ling et al., 2016). However, Neu et al. (2008) used a chemical transport model (CTM) to emphasize that oceanic C_1-C_2 $RONO_2$ may act as a natural source of NO_x via photolysis, increasing the levels of O_3 in the tropical oceanic regions. The coupling effects of $RONO_2$ from photochemical formation and oceanic emissions on O_3 have not been explicitly investigated. In this study, we clearly demonstrate the importance of oceanic contribution to $RONO_2$ especially $MeONO_2$ in coastal region. When future studies focus on the relationship between O_3 and $RONO_2$ during both pollution and non-pollution periods in coastal area, the contribution of photochemical formation versus oceanic emissions has to be taken into account. In order to improve the accuracy of O_3 prediction in coastal environment, the relative contribution of $RONO_2$ from oceanic emissions should be used as an input parameter in photochemical models.

4. Conclusions

Measurements of C_1-C_4 $RONO_2$ were conducted at HKUST, a coastal site in Hong Kong in four selected months of 2011 and 2012. The seasonal variations of C_3-C_4 $RONO_2$ were characterized with higher levels in winter than in summer, while the levels of $MeONO_2$ were significantly higher in summer than those in winter. Receptor models (PCA and PMF) both suggest that photochemical formation and biomass burning were the major sources of C_2-C_4 $RONO_2$, whereas $MeONO_2$ was mainly from oceanic emissions during the entire sampling period. The enrichment of $MeONO_2$ over C_3-C_4 $RONO_2$ was observed in a summer episode when the air masses are mostly derived from the SCS. More important role of oceanic emissions than photochemical formation is suggested in the relative contribution to $RONO_2$ especially $MeONO_2$ in this episode. Due to the limited observation, more intensive field measurements are necessary to assess the sources of $RONO_2$. Besides, comprehensive photochemical models coupled with the relative contribution of $RONO_2$ from oceanic emissions may improve the current understanding of the impact of $RONO_2$ on O_3 production.

Acknowledgements

This study was supported by the National Natural Scientific Foundation of China (Grant No. 41275730 and 41575115, Research Grants Council of Hong Kong Government (PolyU 152083/14E and PolyU 152090/15E) and Hong Kong RGC Collaborative Research Fund (C5022-14G).

We thank the group of Prof. Donald Blake (UCI) for laboratory analysis of the whole air samples. The authors thank HKEPD for provision of the data sets and permission for publication and also thank HKUST's ENVF Atmospheric and Environmental Database for the provision of O_3 and NO_x data sets.

Appendix A. Supplementary data

Supplementary data related to this article can be found at https://doi.org/10.1016/j.chemosphere.2017.11.104.

References

Arey, J., Aschmann, S.M., Kwok, E.S.C., Atkinson, R., 2001. Alkyl nitrate, hydroxyalkyl nitrate, and hydroxycarbonyl formation from the NO_x-air photooxidations of C_5-C_8 *n*-alkanes. J. Phys. Chem. A 105, 1020–1027.

Aruffo, E., Di Carlo, P., Dari-Salisburgo, C., Biancofiore, F., Giammaria, F., Busilacchio, M., Lee, J., Moller, S., Hopkins, J., Punjabi, S., Bauguitte, S., O'Sullivan, D., Percival, C., Le Breton, M., Muller, J., Jones, R., Forster, G., Reeves, C., Heard, D., Walker, H., Ingham, T., Vaughan, S., Stone, D., 2014. Aircraft observations of the lower troposphere above a megacity: alkyl nitrate and ozone chemistry. Atmos. Environ. 94, 479–488.

Atkinson, R., 1997. Gas-phase tropospheric chemistry of volatile organic compounds .1. Alkanes and alkenes. J. Phys. Chem. Ref. Data 26, 215–290.

Atkinson, R., Aschmann, S.M., Carter, W.P.L., Winer, A.M., Pitts, J.N., 1982. Alkyl nitrate formation from the nitrogen oxide NO_x-air photooxidations of C_2-C_8 *n*-alkanes. J. Phys. Chem. 86, 4563–4569.

Atkinson, R., Baulch, D.L., Cox, R.A., Crowley, J.N., Hampson, R.F., Hynes, R.G., Jenkin, M.E., Rossi, M.J., Troe, J., 2006. Evaluated kinetic and photochemical data for atmospheric chemistry: volume II - gas phase reactions of organic species. Atmos. Chem. Phys. 6, 3625–4055.

Atkinson, R., Carter, W.P.L., Winer, A.M., 1983. Effects of temperature and pressure on alkyl nitrate yields in the nitrogen oxide (NO_x) photooxidations of *n*-pentane and *n*-heptane. J. Phys. Chem. 87, 2012–2018.

Atlas, E., 1988. Evidence for $\geq C_3$ alkyl nitrates in rural and remote atmospheres. Nature 331, 426–428.

Atlas, E., Pollock, W., Greenberg, J., Heidt, L., Thompson, A.M., 1993. Alkyl nitrates, nonmethane hydrocarbons, and halocarbon gases over the equatorial Pacific Ocean during SAGA 3. J. Geophys. Res. Atmos. 98, 16933–16947.

Barletta, B., Meinardi, S., Simpson, I.J., Khwaja, H.A., Blake, D.R., Rowland, F.S., 2002. Mixing ratios of volatile organic compounds (VOCs) in the atmosphere of Karachi, Pakistan. Atmos. Environ. 36, 3429–3443.

Barnes, I., Hjorth, J., Mihalopoulos, N., 2006. Dimethyl sulfide and dimethyl sulfoxide and their oxidation in the atmosphere. Chem. Rev. 106, 940–975.

Bertman, S.B., Roberts, J.M., Parrish, D.D., Buhr, M.P., Goldan, P.D., Kuster, W.C., Fehsenfeld, F.C., Montzka, S.A., Westberg, H., 1995. Evolution of alkyl nitrates with air mass age. J. Geophys. Res. Atmos. 100, 22805–22813.

Blake, N.J., Blake, D.R., Swanson, A.L., Atlas, E., Flocke, F., Rowland, F.S., 2003. Latitudinal, vertical, and seasonal variations of C_1-C_4 alkyl nitrates in the troposphere over the Pacific Ocean during PEM-Tropics A and B: oceanic and continental sources. J. Geophys. Res. Atmos. 108, 171–181.

Cheng, Y., Lee, S.C., Huang, Y., Ho, K.F., Ho, S.S.H., Yau, P.S., Louie, P.K.K., Zhang, R.J., 2014. Diurnal and seasonal trends of carbonyl compounds in roadside, urban, and suburban environment of Hong Kong. Atmos. Environ 89, 43–51.

Cheung, K., Ling, Z.H., Wang, D.W., Wang, Y., Guo, H., Lee, B., Li, Y.J., Chan, C.K., 2015. Characterization and source identification of sub-micron particles at the HKUST Supersite in Hong Kong. Sci. Total Environ. 527–528, 287–296.

Chuck, A.L., Turner, S.M., Liss, P.S., 2002. Direct evidence for a marine source of C_1 and C_2 alkyl nitrates. Science 297, 1151–1154.

Clemitshaw, K.C., Williams, J., Rattigan, O.V., Shallcross, D.E., Law, K.S., Cox, R.A., 1997. Gas-phase ultraviolet absorption cross-sections and atmospheric lifetimes of several C_2-C_5 alkyl nitrates. J. Photochem. Photobiol. A Chem. 102, 117–126.

Colman, J.J., Swanson, A.L., Meinardi, S., Sive, B.C., Blake, D.R., Rowland, F.S., 2001. Description of the analysis of a wide range of volatile organic compounds in whole air samples collected during PEM-Tropics A and B. Anal. Chem. 73, 3723–3731.

Dahl, E.E., Yvon-Lewis, S.A., Saltzman, E.S., 2007. Alkyl nitrate (C_1-C_3) depth profiles in the tropical Pacific Ocean. J. Geophys. Res. Oceans 112, 141–143.

Day, D.A., Dillon, M.B., Wooldridge, P.J., Thornton, J.A., Rosen, R.S., Wood, E.C., Cohen, R.C., 2003. On alkyl nitrates, O_3, and the "missing NO_y". J. Geophys. Res. Atmos. 108, 4501.

Ding, A., Wang, T., Zhao, M., Wang, T., Li, Z.K., 2004. Simulation of sea-land breezes and a discussion of their implications on the transport of air pollution during a multi-day ozone episode in the Pearl River Delta of China. Atmos. Environ. 38, 6737–6750.

Fan, S.M., Jacob, D.J., Mauzerall, D.L., Bradshaw, J.D., Sandholm, S.T., Blake, D.R., Singh, H.B., Talbot, R.W., Gregory, G.L., Sachse, G.W., 1994. Origin of tropospheric NO_x over subarctic eastern Canada in summer. J. Geophys. Res. Atmos. 99, 16867–16877.

Flocke, F., Atlas, E., Madronich, S., Schauffler, S.M., Aikin, K., Margitan, J.J., Bui, T.P., 1998a. Observations of methyl nitrate in the lower stratosphere during STRAT: implications for its gas phase production mechanisms. Geophys. Res. Lett. 25, 1891–1894.

Flocke, F., Volz-Thomas, A., Buers, H.J., Patz, W., Garthe, H.J., Kley, D., 1998b. Long-term measurements of alkyl nitrates in southern Germany 1. General behavior and seasonal and diurnal variation. J. Geophys. Res. Atmos. 103, 5729–5746.

Guo, H., Lee, S.C., Louie, P.K.K., Ho, K.F., 2004. Characterization of hydrocarbons, halocarbons and carbonyls in the atmosphere of Hong Kong. Chemosphere 57, 1363–1372.

Guo, H., So, K.L., Simpson, I.J., Barletta, B., Meinardi, S., Blake, D.R., 2007. C_1-C_8 volatile organic compounds in the atmosphere of Hong Kong: overview of atmospheric processing and source apportionment. Atmos. Environ. 41, 1456–1472.

Hofzumahaus, A., Rohrer, F., Lu, K.D., Bohn, B., Brauers, T., Chang, C.C., Fuchs, H., Holland, F., Kita, K., Kondo, Y., Li, X., Lou, S.R., Shao, M., Zeng, L.M., Wahner, A., Zhang, Y.H., 2009. Amplified trace gas removal in the troposphere. Science 324, 1702–1704.

Huang, Y., Ling, Z.H., Lee, S.C., Ho, S.S.H., Cao, J.J., Blake, D.R., Cheng, Y., Lai, S.C., Ho, K.F., Gao, Y., 2015. Characterization of volatile organic compounds at a roadside environment in Hong Kong: an investigation of influences after air pollution control strategies. Atmos. Environ. 122, 809–818.

Iraci, L.T., Riffel, B.G., Robinson, C.B., Michelsen, R.R., Stephenson, R.M., 2007. The acid catalyzed nitration of methanol: formation of methyl nitrate via aerosol chemistry. J. Atmos. Chem. 58, 253–266.

Khan, M.A.H., Cooke, M.C., Utembe, S.R., Morris, W.C., Archibald, A.T., Derwent, R.G., Jenkin, M.E., Orr-Ewing, A.J., Higgins, C.M., Percival, C.J., Leather, K.E., Shallcross, D.E., 2015. Global modeling of the C_1-C_3 alkyl nitrates using STOCHEM-CRI. Atmos. Environ. 123, 256–267.

Kwok, E.S.C., Atkinson, R., 1995. Estimation of hydroxyl radical reaction rate constants for gas-phase organic compounds using a structure-reactivity relationship: an update. Atmos. Environ. 29, 1685–1695.

Lai, S., Zhao, Y., Ding, A., Zhang, Y., Song, T., Zheng, J., Ho, K.F., Lee, S.C., Zhong, L., 2016. Characterization of $PM_{2.5}$ and the major chemical components during a 1-year campaign in rural Guangzhou, Southern China. Atmos. Res. 167, 208–215.

Lai, S.C., Baker, A.K., Schuck, T.J., Slemr, F., Brenninkmeijer, C.A.M., Velthoven, P.V., Oram, D.E., Zahn, A., Ziereis, H., 2011. Characterization and source regions of 51 high-co events observed during civil aircraft for the regular investigation of the atmosphere based on an instrument container (CARIBIC) flights between south China and the Philippines, 2005–2008. J. Geophys. Res. Atmos. 116, 1–15.

Lai, S.C., Baker, A.K., Schuck, T.J., van Velthoven, P., Oram, D.E., Zahn, A., Hermann, M., Weigelt, A., Slemr, F., Brenninkmeijer, C.A.M., Ziereis, H., 2010. Pollution events observed during CARIBIC flights in the upper troposphere between South China and the Philippines. Atmos. Chem. Phys. 10, 1649–1660.

Lai, S.C., Song, J.W., Song, T.L., Huang, Z.J., Zhang, Y.Y., Zhao, Y., Liu, G.C., Zheng, J.Y., Mi, W.Y., Tang, J.H., Zou, S.C., Ebinghaus, R., Xie, Z.Y., 2016. Neutral polyfluoroalkyl substances in the atmosphere over the northern South China Sea. Environ. Pollut 214, 449–455.

Lee, S.C., Chiu, M.Y., Ho, K.F., Zou, S.C., Wang, X.M., 2002. Volatile organic compounds (VOCs) in urban atmosphere of Hong Kong. Chemosphere 48, 375–382.

Ling, Z., Guo, H., Simpson, I.J., Saunders, S.M., Lam, S.H.M., Lyu, X., Blake, D.R., 2016. New insight into the spatiotemporal variability and source apportionments of C_1-C_4 alkyl nitrates in Hong Kong. Atmos. Chem. Phys. 16, 8141–8156.

Ling, Z.H., Zhao, J., Fan, S.J., Wang, X.M., 2017. Sources of formaldehyde and their contributions to photochemical O_3 formation at an urban site in the Pearl River Delta, Southern China. Chemosphere 168, 1293–1301.

Lyu, X.P., Guo, H., Wang, N., Simpson, I.J., Cheng, H.R., Zeng, L.W., Saunders, S.M., Lam, S.H.M., Meinardi, S., Blake, D.R., 2017. Modeling C_1-C_4 alkyl nitrate photochemistry and their impacts on O_3 production in urban and suburban environments of Hong Kong. J. Geophys. Res. Atmos. 122, 10539–10556.

Lyu, X.P., Ling, Z.H., Guo, H., Saunders, S.M., Lam, S.H.M., Wang, N., Wang, Y., Liu, M., Wang, T., 2015. Re-examination of C_1-C_5 alkyl nitrates in Hong Kong using an observation-based model. Atmos. Environ. 120, 28–37.

Man, H.Y., Zhu, Y.J., Ji, F., Yao, X.H., Lau, N.T., Li, Y.J., Lee, B.P., Chan, C.K., 2015. Comparison of daytime and nighttime new particle growth at the HKUST supersite in Hong Kong. Environ. Sci. Technol. 49, 7170–7178.

Moore, R.M., Blough, N.V., 2002. A marine source of methyl nitrate. Geophys. Res. Lett. 29, 27–21-27-24.

Neu, J.L., Lawler, M.J., Prather, M.J., Saltzman, E.S., 2008. Oceanic alkyl nitrates as a natural source of tropospheric ozone. Geophys. Res. Lett. 35, 344–349.

Nowak, J.B., Davis, D.D., Chen, G., Eisele, F.L., Mauldin, R.L., Tanner, D.J., Cantrell, C., Kosciuch, E., Bandy, A., Thornton, D., Clarke, A., 2001. Airborne observations of DMSO, DMS, and OH at marine Tropical latitudes. Geophys. Res. Lett. 28, 2201–2204.

Orlando, J.J., Tyndall, G.S., Calvert, J.G., 1992. Thermal decomposition pathways for peroxyacetyl nitrate (PAN): implications for atmospheric methyl nitrate levels. Atmos. Environ. 26, 3111–3118.

Ou, J.M., Yuan, Z.B., Zheng, J.Y., Huang, Z.J., Shao, M., Li, Z.K., Huang, X.B., Guo, H., Louie, P.K.K., 2016. Ambient ozone control in a photochemically active region: short term despiking or long-term attainment? Environ. Sci. Technol. 50, 5720–5728.

Perring, A.E., Pusede, S.E., Cohen, R.C., 2013. An observational perspective on the atmospheric impacts of alkyl and multifunctional nitrates on ozone and secondary organic aerosol. Chem. Rev. 113, 5848–5870.

Rasmussen, R.A., Rasmussen, L.E., Khalil, M.A.K., Dalluge, R.W., 1980. Concentration distribution of methyl chloride in the atmosphere. J. Geophys. Res. Oceans 85, 7350–7356.

Reeves, C.E., Slemr, J., Oram, D.E., Worton, D., Penkett, S.A., Stewart, D.J., Purvis, R., Watson, N., Hopkins, J., Lewis, A., Methven, J., Blake, D.R., Atlas, E., 2007. Alkyl nitrates in outflow from North America over the North Atlantic during intercontinental transport of ozone and precursors 2004. J. Geophys. Res. Atmos. 112, 409–427.

Roberts, J.M., Bertman, S.B., Parrish, D.D., Fehsenfeld, F.C., Jobson, B.T., Niki, H., 1998. Measurement of alkyl nitrates at chebogue point, nova scotia during the 1993 North Atlantic regional experiment (NARE) intensive. J. Geophys. Res. Atmos. 103, 13569–13580.

Russo, R.S., Zhou, Y., Haase, K.B., Wingenter, O.W., Frinak, E.K., Mao, H., Talbot, R.W., Sive, B.C., 2010. Temporal variability, sources, and sinks of C_1-C_5 alkyl nitrates in coastal New England. Atmos. Chem. Phys. 10, 1865–1883.

Schneider, M., Ballschmiter, K., 1999. C_3-C_{14} alkyl nitrates in remote South Atlantic air. Chemosphere 38, 233–244.

Shepson, P.B., Anlauf, K.G., Bottenheim, J.W., Wiebe, H.A., Gao, N., Muthuramu, K., Mackay, G.I., 1993. Alkyl nitrates and their contribution to reactive nitrogen at a rural site in Ontario. Atmos. Environ. A 27, 749–757.

Simpson, I.J., Akagi, S.K., Barletta, B., Blake, N.J., Choi, Y., Diskin, G.S., Fried, A., Fuelberg, H.E., Meinardi, S., Rowland, F.S., Vay, S.A., Weinheimer, A.J., Wennberg, P.O., Wiebring, P., Wisthaler, A., Yang, M., Yokelson, R.J., Blake, D.R., 2011. Boreal forest fire emissions in fresh Canadian smoke plumes: C_1-C_{10} volatile organic compounds (VOCs), CO_2, CO, NO_2, NO, HCN and CH_3CN. Atmos. Chem. Phys. 11, 6445–6463.

Simpson, I.J., Blake, N.J., Blake, D.R., Atlas, E., Flocke, F., Crawford, J.H., Fuelberg, H.E., Kiley, C.M., Meinardi, S., Rowland, F.S., 2003. Photochemical production and evolution of selected C_2-C_5 alkyl nitrates in tropospheric air influenced by Asian outflow. J. Geophys. Res. Atmos. 108, 8808.

Simpson, I.J., Meinardi, S., Blake, D.R., Blake, N.J., Rowland, F.S., Atlas, E., Flocke, F., 2002. A biomass burning source of C_1-C_4 alkyl nitrates. Geophys. Res. Lett. 29, 21–21-27-24.

Simpson, I.J., Wang, T., Guo, H., Kwok, Y.H., Flocke, F., Atlas, E., Meinardi, S., Rowland, F.S., Blake, D.R., 2006. Long-term atmospheric measurements of C_1-C_5 alkyl nitrates in the pearl river delta region of Southeast China. Atmos. Environ. 40, 1619–1632.

Smyth, S., Bradshaw, J., Sandholm, S., Liu, S., Mckeen, S., Gregory, G., Anderson, B., Talbot, R., Blake, D., Rowland, S., 1996. Comparison of free tropospheric western Pacific air mass classification schemes for the PEM-West A experiment. J. Geophys. Res. Atmos. 101, 1743–1762.

Song, T.L., Wang, S., Zhang, Y.Y., Song, J.W., Liu, F.B., Fu, P.Q., Shiraiwa, M., Xie, Z.Y., Yue, D.L., Zhong, L.J., Zheng, J.Y., Lai, S.C., 2017. Proteins and amino acids in fine particulate matter in rural Guangzhou, Southern China: seasonal cycles, sources, and atmospheric processes. Environ. Sci. Technol 51, 6773–6781.

Stein, A.F., Draxler, R.R., Rolph, G.D., Stunder, B.J.B., Cohen, M.D., Ngan, F., 2015. Noaa's hysplit atmospheric transport and dispersion modeling system. Bull. Am. Meteorol. Soc. 96, 2059–2077.

Talukdar, R.K., Burkholder, J.B., Hunter, M., Gilles, M.K., Roberts, J.M., Ravishankara, A.R., 1997a. Atmospheric fate of several alkyl nitrates. 2. UV absorption cross-sections and photodissociation quantum yields. J. Chem. Soc. Faraday Trans. 93, 2797–2805.

Talukdar, R.K., Herndon, S.C., Burkholder, J.B., Roberts, J.M., Ravishankara, A.R., 1997b. Atmospheric fate of several alkyl nitrates. 1. Rate coefficients of the reactions alkyl nitrates with isotopically labelled hydroxyl radicals. J. Chem. Soc. Faraday Trans. 93, 2787–2796.

Wang, M., Shao, M., Chen, W.T., Lu, S.H., Wang, C., Huang, D.K., Yuan, B., Zeng, L.M., Zhao, Y., 2013. Measurements of C_1-C_4 alkyl nitrates and their relationships with carbonyl compounds and O_3 in Chinese cities. Atmos. Environ. 81, 389–398.

Wang, T., Ding, A.J., Blake, D.R., Zahorowski, W., Poon, C.N., Li, Y.S., 2003. Chemical characterization of the boundary layer outflow of air pollution to Hong Kong during February-April 2001. J. Geophys. Res. Atmos. 108, 251–261.

Williams, J.E., Le Bras, G., Kukui, A., Ziereis, H., Brenninkmeijer, C.A.M., 2014. The impact of the chemical production of methyl nitrate from the NO + CH_3O_2 reaction on the global distributions of alkyl nitrates, nitrogen oxides and tropospheric ozone: a global modelling study. Atmos. Chem. Phys. 14, 2363–2382.

Worton, D.R., Reeves, C.E., Penkett, S.A., Sturges, W.T., Slemr, J., Oram, D.E., Bandy, B.J., Bloss, W.J., Carslaw, N., Davey, J., Emmerson, K.M., Gravestock, T.J., Hamilton, J.F., Heard, D.E., Hopkins, J.R., Hulse, A., Ingram, T., Jacob, M.J., Lee, J.D., Leigh, R.J., Lewis, A.C., Monks, P.S., Smith, S.C., 2010. Alkyl nitrate photochemistry during the tropospheric organic chemistry experiment. Atmos. Environ. 44, 773–785.

Wu, Z.Y., Wang, X.M., Chen, F., Turnipseed, A.A., Guenther, A.B., Niyogi, D., Charusombat, U., Xia, B.C., Munger, J.W., Alapaty, K., 2011. Evaluating the calculated dry deposition velocities of reactive nitrogen oxides and ozone from two community models over a temperate deciduous forest. Atmos. Environ. 45, 2663–2674.

Xu, Z., Xue, L.K., Wang, T., Xia, T., Gao, Y., Louie, P.K.K., Luk, C.W.Y., 2015. Measurements of peroxyacetyl nitrate at a background site in the Pearl River delta region: production efficiency and regional transport. Aerosol Air Qual. Res. 15, 833–841.